Reactive Transport Modelling of Fluid-NCG Reinjection in Ngā Tamariki Geothermal Field

Yeftamikha Siahaan[1], Eylem Kaya[1], Dale E. Altar[1], John Mering[2], Denni Subekti[2], Ayu Utami[2], Roxanne Atayde[2], Kelly Melia[2], Fabian Sepulveda[2]

[1]University of Auckland, New Zealand

[2]Mercury Energy Ltd., New Zealand

yyef541@aucklanduni.ac.nz

Keywords: *reactive transport model, TOUGHREACT, NCG reinjection, Ngā Tamariki.*

ABSTRACT

As global efforts intensify to realise a carbon-neutral future, the reinjection of non-condensable gases (NCG) into geothermal fields offers a promising option to reduce greenhouse gas emissions. The ongoing CO_2 reinjection program at Ngā Tamariki, which has been operational since October 2021, reinjects NCG from one of the binary units, reducing annual GHG emissions from the station by 25% (>8,000tCO_2e p.a.).

To provide quantitative insights into the geothermal reservoir response at Ngā Tamariki under various NCG reinjection conditions, and to assess mineral reactions and geochemical processes, 2D reactive transport modelling was conducted using TOUGHREACT v.4.13. The models aim to identify major precipitation and dissolution reactions of minerals and their long-term impacts on permeability and the flow paths, elucidate the fate of reinjected NCGs and explore CO_2 trapping mechanisms for sequestration. By simulating both injection and production behaviour within the reservoir, the models examine the relationship between these and provide insights into geochemical alteration resulting from changes in the thermodynamic conditions.

Based on the 2D model, an increase of NCG reinjection from 0% to 25% of the total NCG of the plants widened the area of porosity-permeability enhancement, along with increased calcite and anhydrite dissolution, and reduced precipitation of pyrite. However, further increasing NCG reinjection from 25% to 50% was insignificant in terms of changes in porosity-permeability or the amount of anhydrite or pyrite. Only calcite exhibits a more widespread and enhanced dissolution response at the increased NCG reinjection rate.

1. INTRODUCTION

As a low-emission and base-load renewable energy source, geothermal energy plays an important role in the transition to a low-carbon future. Geothermal power is considered clean, with significantly lower emissions compared to fossil fuels (Mclean & Richardson, 2019). The emissions from geothermal power plants primarily consist of non-condensable gases (NCGs) such as CO_2, CH_4, H_2S, NH_3, N_2, and H_2, which are naturally formed in the reservoir (Nicholson, 1993).

NCG emissions from geothermal operations can be decreased via reinjection into the reservoir. This NCG injection might positively impact reservoir recharge, pressure support, and steam production (Kaya & Zarrouk, 2017). However, NCG injection introduces technical challenges that vary by plant type and field characteristics. Relevant questions to NCG injection include the degree of NCG breakthrough to adjacent production wells, the likelihood of leakage to the surface through faults and fractures, or the potential for changes in porosity, permeability, and strength of the reservoir rock.

The combination of NCG and geothermal wastewater reinjection, together with subsequent changes in the reservoir fluid chemistry, pH, and thermodynamic conditions can lead to both mineral dissolution and the formation of new minerals in the surrounding formation, potentially affecting the flow dynamics. Reactive transport models are essential for understanding potential changes in the reservoir due to mineralogical formation and dissolution. Such changes can be used to predict alterations in flow paths, and the overall impact on the capacity of injection and nearby production wells.

The Ngā Tamariki geothermal field is located in the Taupo Volcanic Zone (Figure 1). Ngā Tamariki power station consists of four identical OEC (Ormat Energy Converter) units. Since mid-October 2021, a pilot NCG reinjection system has been in place to inject emissions from one of these four units, successfully implementing NCG reinjection. This trial achieved a reduction of 10,000 tonnes of CO_2e per year, representing a 25% reduction in Ngā Tamariki emissions. Expansion at the Ngā Tamariki power station is ongoing, with Mercury Energy Ltd aiming for an 80% reduction in emissions by 2026 (NZGA CO_2 Workshop, 2024).

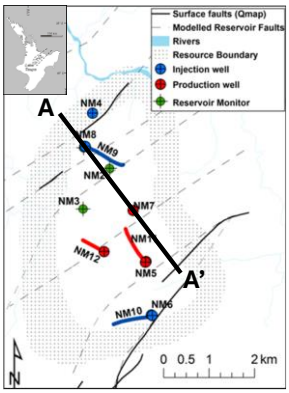

Figure 1: Ngā Tamariki geothermal field with the location of the wells (Quinao et al., 2017). Line A-A' is the focus area of this model.

As reported by Abd Ghafar et al. (2022), after almost one year of operation, no adverse impacts have been observed in either the adjacent production well or the reinjection wells.

Reactive transport modelling offers a valuable tool to evaluate the current condition and estimate the long-term effect of the NCG reinjection on the reservoir. It should be noted that uncertainties are expected due to model parameter assumptions, the availability of data, and the representation

ISSN 2703-4275

of the complex interactions between chemical reactions and flow dynamics, all of which can significantly impact the accuracy of the model predictions. This paper presents the result of a 2D reactive transport model, building on the findings of the 1D-radial model discussed in Siahaan et al. (2024). By enhancing the model structure, we aim to explore the interactions between production and injection wells and improve the estimation of fluid movement. The study provides quantitative insights into the reservoir and formation responses under various NCG injection conditions. It focuses on reaction mechanisms under the reservoir's thermophysical and thermodynamic conditions, potentially leading to more efficient and sustainable CO_2 injection and storage techniques in geothermal fields.

2. METHODOLOGY

2.1 Reactive Transport Model Setup and Parameters

2.1.1 Reactive transport model

The reactive transport model utilised in this project was constructed using TOUGHREACT v.4.13 (Sonnenthal et al., 2021), employing the EOS1 fluid equation of state, which is suitable for hydrothermal systems and provides properties for pure water. TOUGHREACT is a programme for conducting numerical simulations with the capability to simulate chemically reactive non-isothermal multiphase flow fluids in porous and fractured rock formations (Xu et al., 2006). It was developed by incorporating geochemical conditions into the TOUGH2 simulator, enhancing its capability to model the interactions between fluids and rock matrices in complex geological systems. Numerous subsurface thermophysical and chemical processes are considered across a broad range of temperature, pressure, ionic strength, water saturation, pH, and Eh conditions. Mineral and fluid interaction can occur under equilibrium conditions or with kinetic rates. The simulation can be used to predict how the porosity and permeability of the formation change over time based on the precipitation and dissolution processes.

PyTOUGH (Croucher, 2023) was used for creating the model grids, transferring the initial condition (INCON) and rock properties from Mercury's model to the current study, and visualising the results from TOUGHREACT. TIM (Yeh et al., 2013) was used for visualising the distribution of specific parameters within the grid structure, as can be seen in Figure 2.

2.1.2 Model setup

The model grid was designed to encompass the NM9 and NM8 reinjection wells, northern injection wells currently utilized for continuous NCG reinjection. The model grid also includes the NM7, the closest active production well to both NM8 and NM9. The 2014 tracer test at Ngā Tamariki also suggests the connectivity between NM9 and NM7 (Buscarlet et al., 2015). The model's grid structure can be seen in Figure 2. The vertical extent of the model created ranges from -900 to -3210 mASL to include all the feedzones of the NM9, NM8, and NM7.

The initial conditions (INCON) were aligned with Mercury's 3D numerical model's primary variable distributions (e.g. pressure and temperature), using the same transfer function used to extract the rock-type data in PyTOUGH (Croucher, 2023). Injection and production rates were assigned to the individual grid blocks according to the depth and proportion of feedzones for NM9, NM8, and NM7. The location of the grids with their rate proportion of injection or production can be seen in Figure 2. For each well, the injection and production rates were kept consistent over each period in the modelling scenario, using the average rate for each period. For the future modelling period, the rates were based on the current NCG reinjection period.

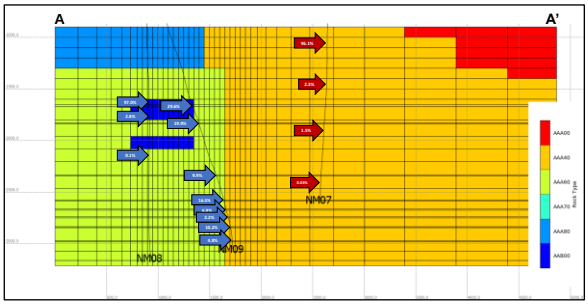

Figure 2: The model grids showing the grid location assigned with injection (blue arrows) and production (red arrows) based on each well's feedzones depth and rate proportion.

2.1.3 Fluid chemistry

The geochemistry data is used as input for the model to incorporate both reservoir and injection fluid chemistry. The reservoir fluid chemistry was determined from the produced fluid from NM7 which was corrected to the reservoir conditions through quartz geothermometer calculations. The reservoir fluid chemistry used in the model can be seen in Table 1. The injection fluid chemistry includes mixed brine, condensate, and NCG chemistry data (summarised in Table 2). PHREEQC (Parkhurst & Appelo, 2013) was used to conduct several chemical calculations. The fluid chemistry used in this 2D model aligns with our 1D-radial model presented in Siahaan et al. (2024).

Table 1: Reservoir fluid chemistry of NM7.

	Concentration (ppm)	
Date	1/15/2019	8/2/2021
Fluid		
pH	6.119	6.149
Na^+	504.6	485.8
Cl^-	842.0	837.4
HCO_3^-	38.2	34.3
Ca^{2+}	2.6	2.6
SO_4^{2-}	7.4	9.0
Mg^{2+}	0.01	0.01
Fe^{2+}	0.01	0.02
K^+	112.6	108.1
$SiO_{2(aq)}$	623.1	642.3
AlO_2^-	0.3	0.2
Gas		
CO_2	2013.5	1904.7
H_2S	38.2	70.4
CH_4	21.5	18.3
H_2	0.1	0.1

Table 2: Injected fluid chemistry with some recalculation for pH and bicarbonate.

	Concentration (ppm)		
	Scenario 1: 0% NCG reinjection	**Scenario 2: 25% NCG reinjection**	**Scenario 3: 50% NCG reinjection**
Fluid			

ISSN 2703-4275

pH	5.52	5.23	5.08
Na^+	501.0	501.0	501.0
Cl^-	931.0	931.0	931.0
HCO_3^-	101.9	101.9	101.9
Ca^{2+}	2.9	2.9	2.9
SO_4^{2-}	10.3	10.3	10.3
Mg^{2+}	0.0	0.0	0.0
Fe^{2+}	0.5	0.5	0.5
K^+	107.0	107.0	107.0
$SiO_{2(aq)}$	688.0	688.0	688.0
AlO_2^-	0.8	0.8	0.8
Gas			
CO_2	533.2	928.6	1324.1
H_2S	66.2	75.1	84.0
CH_4	4.0	8.1	12.2
H_2	0.00001	0.00001	0.00001

2.1.4 Mineral volume fractions and reactive surface areas (RSA)

In the 2D model presented in this paper, we adopted the same mineral volume fraction data as we used in the 1D-radial model (Siahaan et al. 2024). These mineral volume fractions were determined through Tescan Integrated Mineral Analyzer (TIMA) and X-ray Diffraction (XRD) analysis by Sewell (2022), and were supplemented by information from the NM9 geological report by Lewis et al. (2013). The volume fraction of minerals used in the model can be seen in Table 3. It is important to note that, while minerals such as amorphous silica, chalcedony, smectite, and montmorillonite were not initially present in the mineralogy data, they were included in the model input as potential secondary minerals with an initial volume fraction of 0%. This allows us to assess the potential precipitation of these minerals.

The RSA for the minerals was calculated based on the approaches outlined in the TOUGHREACT module for each mineral and both the fracture and matrix domains (Sonnenthal et al., 2021). The RSA values used in the model can be seen in Table 3.

2.1.5 Chemical reaction of minerals

The behaviour of the minerals within the model also depends on the chemical reactions occurring in geothermal systems. Mineral reactions can be assigned as either equilibrium or kinetic. In this model, all minerals were assigned with kinetic constraints. The rate constants, activation energies, and rate laws used for these minerals set in the model can be seen in Table 4. These data were mainly referred to Altar & Kaya (2020), Palandri & Kharaka (2004), and Xu et al. (2007).

The dissolution reactions of each mineral were incorporated into the thermodynamic database. They are useful for identifying which chemical species might influence mineral precipitation or dissolution beyond the reaction parameters stated above. A summary of the chemical species involved in the dissolution reactions of the minerals can be seen in Table 5.

Table 3: Volume fraction and calculated RSA for each mineral.

Minerals	Volume fraction	RSA (m^2/m^3)	RSA/1000
Quartz	50%	1.414E+02	1.414E-01
Albite	2%	5.655E+00	5.655E-03
Calcite	7%	1.979E+01	1.979E-02
Chlorite	2%	5.655E+00	5.655E-03
Pyrite	2%	5.655E+00	5.655E-03
Illite	12%	3.393E+01	3.393E-02
Kaolinite	7%	1.979E+01	1.979E-02
Anhydrite	5%	1.414E+01	1.414E-02
Pyrophyllite	7%	1.979E+01	1.979E-02
Am-silica	0%	3.142E+02	3.142E-01
Chalcedony	0%	3.142E+02	3.142E-01
Smectite	0%	3.142E+02	3.142E-01
Montmorillonite	0%	3.142E+02	3.142E-01
Matrix	-	4.440E+03	-

2.1.6 Model calibration

Several calibration approaches were conducted on the 2D model. Besides the calibration of pressure and chemistry conducted on the 1D-radial model (Siahaan et al., 2024), other calibrations using pressure, temperature, and tracer data were also conducted.

Table 4: Kinetic reaction parameters for minerals consisted of rate constants, activation energies, and rate laws (Altar & Kaya, 2020; Xu et al., 2007; and Palandri & Kharaka, 2004).

Mineral	Dissolution			Precipitation		
	Log k_{25}	E_a	Rate law	Log k25	E_a	Rate law
Quartz	-13.99	87.7		-9.42	49.8	$a_{SiO_{2(aq)}}$
Albite	-10.16	65.0	$a_{H^+}^{0.457}$			
	-12.56	69.8				
	-15.60	71.0	$a_{H^+}^{-0.572}$			
Calcite	-0.30	14.4	a_{H^+}	-2.15	51.9	$a_{Ca^{2+}}a_{HCO_3^-}$
	-5.81	23.5				
Chlorite	-11.11	88.0	$a_{H^+}^{0.5}$			
Pyrite	-4.55	56.9				
Illite	-12.60	14.0				
Kaolinite	-13.18	22.2				
Smectite	-12.78	35.0				
Montmorillonite	-14.41	48.0				
Anhydrite	-3.19	14.3				
Pyrophyllite	-12.40	29.0				
Amorphous silica				-9.42	49.8	$a_{SiO_{2(aq)}}$
Chalcedony				-9.42	49.8	$a_{SiO_{2(aq)}}$

ISSN 2703-4275

Table 5: Summary of chemical species of each mineral's chemical reaction.

Mineral	Chemical species
Albite	Na^+, $SiO_{2(aq)}$, AlO_2^-
Calcite	H^+, Ca^{2+}, HCO_3^-
Chlorite	H^+, $SiO_{2(aq)}$, Fe^{2+}, Mg^{2+}, H_2O, AlO_2^-
Pyrite	$H_{2(aq)}$, H^+, Fe^{2+}, $H_2S_{(aq)}$
Illite	H^+, Mg^{2+}, K^+, $SiO_{2(aq)}$, H_2O, AlO_2^-
Kaolinite	H^+, $SiO_{2(aq)}$, H_2O, AlO_2^-
Anhydrite	Ca^{2+}, SO_4^{2-}
Pyrophyllite	H^+, $SiO_{2(aq)}$, AlO_2^-
Quartz	$SiO_{2(aq)}$
Am-silica	$SiO_{2(aq)}$
Chalcedony	$SiO_{2(aq)}$
Smectite	H_2O, Ca^{2+}, H^+, Mg^{2+}, $SiO_{2(aq)}$, AlO_2^-
Montmorillonite	H^+, Ca^{2+}, K^+, Na^+, Mg^{2+}, H_2O, $SiO_{2(aq)}$, AlO_2^-

Based on the pressure and temperature calibration of the 2D model, it was decided to use only half of the injection and production rate. The reason for this is that this model is a 2D model, which has only one horizontal direction (the x-axis), unlike a 3D model, which has two horizontal directions (the x and y axes). Using the full rate also results in an anomaly of high pressure and cooler temperature in the largest feedzone of NM7.

To represent the hydraulic connection and flow paths between wells more realistically in our 2D model, we also used the data from 2014 tracer test at the Ngā Tamariki geothermal field as a calibration parameter (Buscarlet et al., 2015). This test showed that tracer returns from the southern reinjection well were faster (28 days) compared to the northern reinjection well (100 days). Tracer from NM9 (2,7-NDS) was recovered in NM7, which showed the second-highest recovery rate, suggesting a longer and more complex pathway between these wells.

The tracer test was simulated in the 2D model created for this study, involving the injection of a naphthalene disulfonate tracer and sampling in the production wells. The model was initially run for one day, followed by a restart without tracer injection to analyse the tracer behaviour in NM7's largest feedzone.

Results indicated that 3.5% of the tracer injected in NM9 was recovered in NM7, closely matching the 4.7% recovery observed in the field test. However, there are some discrepancies in the model, particularly in the timing and value of the first tracer arrival and peak. These differences may be due to approximations in the injected tracer concentration and the inherent limitations of the 2D model.

2.2 Model Scenarios

Three NCG reinjection scenarios were modelled: 0% NCG reinjection scenario (Scenario 1), 25% NCG reinjection scenario (Scenario 2), and 50% NCG reinjection scenario (Scenario 3). Each scenario was divided into three different periods: Before NCG reinjection (2013-2021), during current NCG reinjection (2021-2024), and future NCG reinjection (2024-2034). A summary of the scenarios can be seen in Table 6.

Table 6: Scenarios that are being used in the model.

Period	Scenario 1: 0% NCG reinjection	Scenario 2: 25% NCG reinjection	Scenario 3: 50% NCG reinjection
Before NCG reinjection (2013-2021)	No additional NCG injection (only passive)	No additional NCG injection	No additional NCG injection
Current NCG reinjection (2021-2024)		25% NCG injection	25% NCG injection
Future NCG reinjection (2024-2034)			50% NCG injection

3. RESULTS AND DISCUSSION

3.1 Effects on the Mineral Volume Fraction

Overall, the effects on mineral volume fractions in the 2D model are similar to those observed in the 1D-radial model (Siahaan et al., 2024). This section will focus on the trend of several key minerals that show significant changes, namely calcite, anhydrite, and pyrite. Other minerals, such as amorphous silica, quartz, and clay minerals, show less significant changes in the model.

Higher NCG reinjection shows more dissolution of calcite. In Figure 3-A, calcite shows a broader and higher magnitude of dissolution with increasing NCG reinjection. The precipitation area is also only found in a smaller area at the upper part of the model, in contrast to the broader dissolution area. The precipitation at the upper part of the model may be due to the rise of CO_2 in the reservoir.

Similar to calcite, anhydrite also shows more dissolution with a higher NCG reinjection. It can be seen in Figure 3-B that there is a slight expansion of the blue dissolution area with increasing NCG reinjection. However, the NCG reinjection increase from 25% to 50% does not significantly affect anhydrite dissolution, as shown in Figure 3-B.

Pyrite precipitates only in the near reinjection wellbore area, consistent with the results from the 1D-radial model (Siahaan et al., 2024). Figure 3-C also shows that higher NCG reinjection leads to less pyrite precipitation, as shown by the reduced yellow colouration in the 25% and 50% NCG reinjection scenarios. However, the change in pyrite volume fraction between the 25% and 50% NCG reinjection scenarios is insignificant.

In the 2D model, the differences between various NCG reinjection scenarios, especially between 0% and 25% NCG reinjection scenarios, are more pronounced than in the 1D-radial model. Figure 4 shows the example of the results for calcite and anhydrite from the 1D-radial model for comparison (Siahaan et al., 2024). This different trend is visible, especially in the volume fraction changes of calcite, anhydrite, and pyrite. For calcite, the distinction between the 25% and 50% NCG reinjection scenarios is also more evident in the 2D model. The possible reason for this is the dimension limitation of the 1D-radial model, which has only a horizontal dimension compared to the 2D model, which has horizontal and vertical dimensions that can show more visible differences.

ISSN 2703-4275

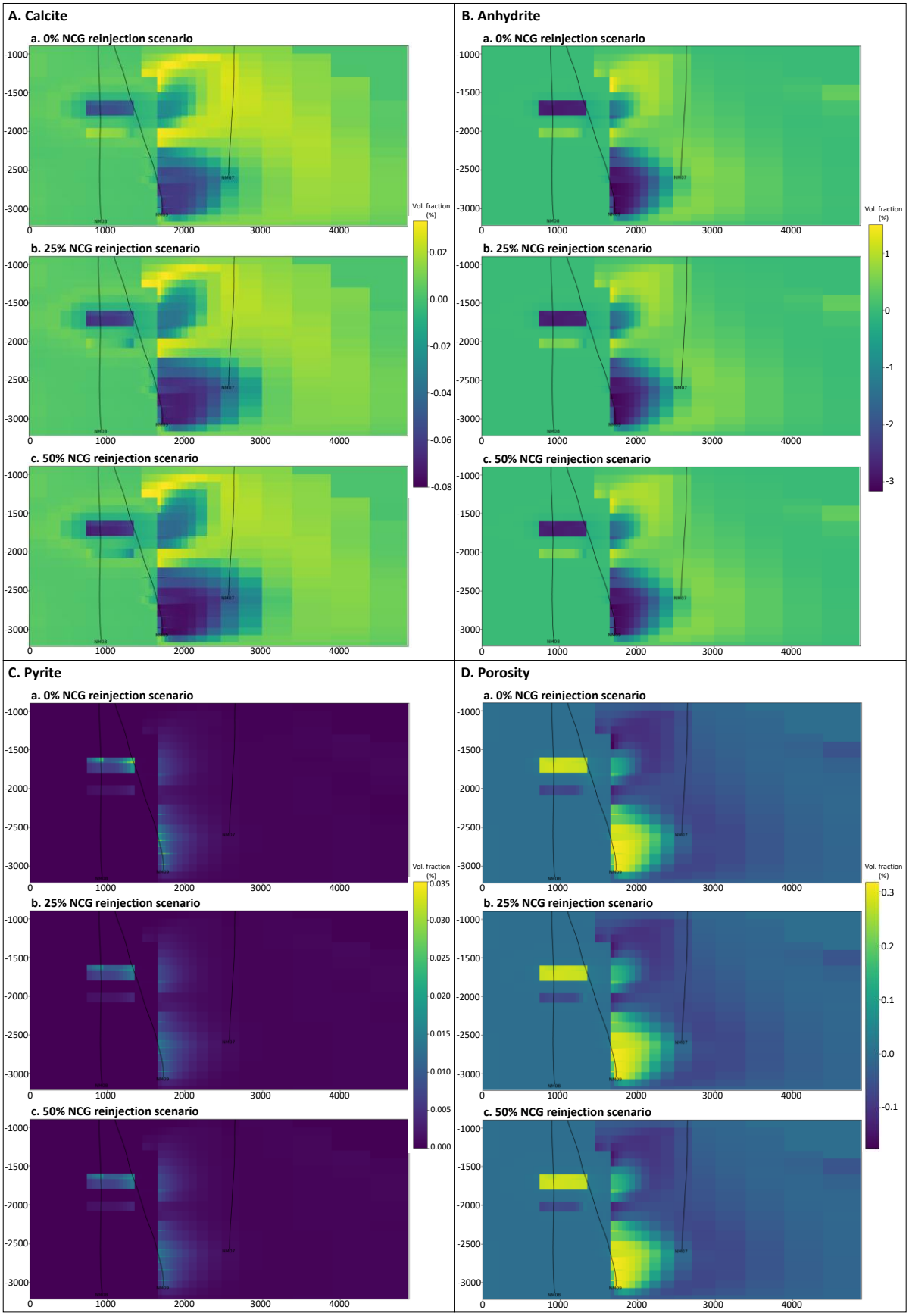

Figure 3: Volume fraction change of calcite (A), anhydrite (B), pyrite (C), and changes of porosity (D) at the end of the model run in 2034. Yellow indicates value increase while blue indicates value decrease or no changes (for pyrite). Higher NCG reinjection shows more calcite and anhydrite dissolution, and less pyrite precipitation, which contributes to an increase in porosity, especially between 0% and 25% NCG reinjection scenarios.

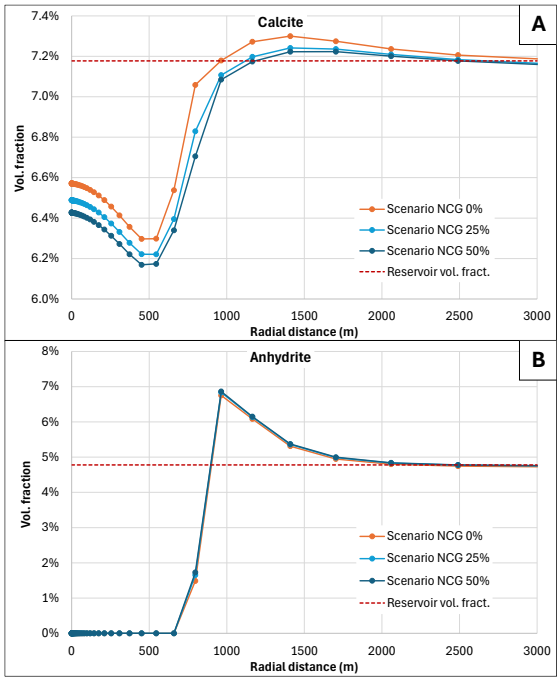

Figure 4: 1D-radial model results of volume fraction change of calcite (A) and anhydrite (B) (Siahaan et al., 2024). The difference between 0% to 25% NCG reinjection scenarios, especially for anhydrite, only shows minimal changes compared to the 2D model.

3.2 Effects on Porosity and Permeability

The simultaneous process of mineral dissolution and precipitation described above leads to changes in the rock's porosity and permeability. The changes of porosity at the end of the model run in 2034 for each NCG reinjection scenario can be seen in Figure 3-D, while the results for permeability show a similar trend, which is not shown in this figure.

The results of the 2D model show that porosity and permeability increase near the reinjection wells while they decrease in the smaller areas in the upper area of the model and further areas from the reinjection wells. An increase in NCG reinjection from 0% to 25% results in a broader area of increased porosity and permeability due to the dissolution of minerals such as anhydrite and calcite. However, the changes in porosity and permeability between 25% and 50% NCG reinjection scenarios are insignificant.

4. CONCLUSION

The reactive transport models effectively capture mineral reactions and their effect on reservoir flow dynamics. This study utilises a 2D field scale model to analyse changes in the geochemical properties of geothermal formations to evaluate the effects of the NCG reinjection on the Ngā Tamariki reservoir. Specifically, the models simulate NCG reinjection into the NM9 and NM8 reinjection wells located in the northern part of the Ngā Tamariki geothermal field. The models also evaluate the effect of this reinjection on the adjacent production well, namely NM7.

In the 2D model, an increase of NCG reinjection from 0% to 25% resulted in an enhanced calcite and anhydrite dissolution, and reduced precipitation of pyrite. These changes in minerals then resulted in a broader area of increased porosity and permeability. However, the increase in NCG reinjection from 25% to 50% was insignificant in terms of changes in porosity, permeability, or the changes in the amount of anhydrite or pyrite mineral abundance. Only calcite exhibited a more widespread and enhanced dissolution response due to increased NCG reinjection from 25% to 50% of the total station emission.

The 2D model also shows a broader area of increased porosity and permeability near the reinjection wells, contrasted with smaller areas of decreased porosity and permeability, mainly in the upper and outer areas of the model.

The work highlights the value of reactive transport modelling in providing detailed insights into the impacts of NCG reinjection on mineralogy, fluid chemistry, and reservoir properties. To comprehensively assess the overall impact of increased NCG reinjection in Ngā Tamariki, a further large-scale 3D modelling study is required. Such a modelling study should incorporate more representative mineralogy variations and boundary conditions and consider the interactions with other production and injection wells. Future investigations should also include longer-term model simulations, a full range of NCG reinjection scenarios, and considerations of structural influences on reservoir flow behaviour.

ACKNOWLEDGEMENTS

The authors would like to thank Mercury Energy Ltd. for providing field data, permission to publish, and for the support and discussions during this research. We also thank the NZ Ministry of Business, Innovation and Employment for funding the work through the MBIE Research Programme: UOAX2211 "Reversing Carbon Emissions in the Geothermal Energy Industry: Template for Emission-Intensive Industries" and GNS-MBIE00150 "Geothermal: The Next Generation" projects.

REFERENCES

Abd Ghafar, S., Allan, G., Ferguson, A., Siega, F., Rivera, M., & Murphy, B. (2022). Non Condensable Gas Reinjection Trial at Ngatamariki Geothermal Power Plant. *Proceedings 44th New Zealand Geothermal Workshop*.

Altar, D. E., & Kaya, E. (2020). Numerical modelling of the interaction between geothermal injectate-non condensable gas solutions and greywacke. *International Journal of Greenhouse Gas Control, 94*. https://doi.org/10.1016/j.ijggc.2019.102922

Buscarlet, E., Moon, H., & Wallis, I. (2015). Reservoir tracer test at the Ngatamariki geothermal field. *Proceedings 37th New Zealand Geothermal Workshop*. https://www.researchgate.net/publication/284392576

Croucher, A. (2023). *PyTOUGH user's guide*.

Kaya, E., & Zarrouk, S. J. (2017). Reinjection of greenhouse gases into geothermal reservoirs. *International Journal of Greenhouse Gas Control, 67*, 111–129. https://doi.org/10.1016/j.ijggc.2017.10.015

Lewis, B., Chambefort, I., Rae, A. J., & Sanders, F. (2013). *Geology of Well NM9, Ngatamariki Geothermal Field.*

Mclean, K., & Richardson, I. (2019, November 23). Greenhouse gas emissions from New Zealand geothermal power generation in context. *Proceedings 38th New Zealand Geothermal Workshop*.

Nicholson, K. (1993). *Geothermal Fluids*. Springer Berlin Heidelberg. https://doi.org/10.1007/978-3-642-77844-5

Palandri, J. L., & Kharaka, Y. K. (2004). *A compilation of rate parameters of water-mineral interaction kinetics for application to geochemical modeling*.

Parkhurst, David. L., & Appelo, C. A. J. (2013). *Description of Input and Examples for PHREEQC Version 3-A Computer Program for Speciation, Batch-Reaction, One-Dimensional Transport, and Inverse Geochemical Calculations*. http://www.hydrochemistry.eu

Quinao, J. J., Buscarlet, E., & Siega, F. (2017, February 13). Early Identification and Management of Calcite Deposition in the Ngatamariki Geothermal Field, New Zealand. *Proceedings 42nd Workshop on Geothermal Reservoir Engineering*. https://www.researchgate.net/publication/313878492

Sewell, S. (2022). *Geologic controls on seismic velocity from well logs and seismic tomography at the Rotokawa and Ngatamariki Geothermal Fields, New Zealand*. Victoria University of Wellington.

Siahaan, Y., Kaya, E., Altar, D. E., Mering, J., Subekti, D., Utami, A., Atayde, R., Melia, K., & Sepulveda, F. (2024). Modelling non-condensable gas reinjection geochemical dynamics in geothermal fields: a case study of Ngā Tamariki, New Zealand. *PROCEEDINGS, The 10th Indonesia International Geothermal Convention & Exhibition (IIGCE) 2024*.

Sonnenthal, E., Spycher, N., Xu, T., & Zheng, L. (2021). *TOUGHREACT V4.13-OMP & TReactMech V1.0*.

Xu, T., Apps, J. A., Pruess, K., & Yamamoto, H. (2007). Numerical modeling of injection and mineral trapping of CO2 with H2S and SO2 in a sandstone formation. *Chemical Geology*, *242*(3–4), 319–346. https://doi.org/10.1016/j.chemgeo.2007.03.022

Xu, T., Sonnenthal, E., Spycher, N., & Pruess, K. (2006). TOUGHREACT - A simulation program for non-isothermal multiphase reactive geochemical transport in variably saturated geologic media: Applications to geothermal injectivity and CO2 geological sequestration. *Computers and Geosciences*, *32*(2), 145–165. https://doi.org/10.1016/j.cageo.2005.06.014

Yeh, A., Croucher, A. E., & O'Sullivan, M. J. (2013). TIM-yet another graphical tool for TOUGH2. *35th New Zealand Geothermal Workshop*.

ISSN 2703-4275